

---

**Interactive comment on “Observations and explicit modeling of isoprene chemical processing in polluted air masses in rural areas of the Yangtze River Delta region: radical cycling and formation of ozone and formaldehyde” by Kun Zhang et al.**

**Response to Referee #1**

Received and published: 29 September 2020

Major comments

I find two main issues with the analysis presented in sections 3.2 and 3.3. One is the lack of heterogeneous chemistry in the model. This is likely to impact both the levels and the budget of OH (because of the heterogeneous sources of HONO), of HO<sub>2</sub> (because of HO<sub>2</sub> uptake on aerosol), and of NO<sub>3</sub> (because of the equilibrium with N<sub>2</sub>O<sub>5</sub>). I don't think that a complete analysis of radical chemistry can just ignore these processes. If the authors think that heterogeneous chemistry is negligible under the conditions of this study (and it may well be so), they should provide some evidence or reason why that is the case.

Response: We really appreciate the reviewers careful and valuable comments. We agree that the heterogeneous processes associated with HONO source, uptake of HO<sub>2</sub> and N<sub>2</sub>O<sub>5</sub> could be important for the budget of OH, HO<sub>2</sub> and NO<sub>3</sub> under certain conditions. Therefore, we tested the heterogeneous processes including uptake of N<sub>2</sub>O<sub>5</sub>, HCHO, and HO<sub>2</sub> on aerosols surface, and heterogenous sources of HONO in our simulation, as summarized in Table 1. Rate constants and uptake coefficients for these reactions were obtained from previous studies (Riedel et al. (2014); Xue et al. (2014); Li et al. (2014)). Since key parameters such as aerosol surface areas ( $S_A$ ) were not directly measured during our observation period, an average value of  $S_A$  (640 nm<sup>2</sup>/cm<sup>3</sup> from the study of Wang et al. (2014)) was adopted in this study. Our results suggest that adding heterogenous processes in our simulation could lead to decrease of OH, HO<sub>2</sub>, RO<sub>2</sub> and NO<sub>3</sub> by 1.53%, 4.54%, 2.73%

and 6.53%, respectively. These processes have been included in our base simulation and results are updated accordingly.

Table 1. Additional heterogenous reactions and associated rate constants used by the model

Reactions	Rate constants	No.
$N_2O_5 \rightarrow CLNO_2 + HNO_3$	$\gamma\omega S_A/4$ (for $CLNO_2$ formation) $(2 - \phi)\gamma\omega S_A/4$ (for $HNO_3$ formation)	Riedel et al. (2014)
$NO_2 \rightarrow HONO$	$k_g = \frac{1}{8} \times \omega\gamma\left(\frac{S}{V}\right)$ $k_a = \frac{1}{4} \omega\gamma S_A$	Xue et al. (2014)
$HO_2 \rightarrow products$	$k = \left(\frac{r}{D_g} - \frac{4}{\gamma}\omega\right)^{-1} S_A$	Xue et al. (2014)
$HCHO \rightarrow products$	$k = \frac{1}{4} \omega\gamma S_A$	Li et al. (2014)

$\gamma$ = uptake coefficient for the given reactant with aerosol surface area;  $\phi$  = product yield;  $\omega$ =mean molecular speed of the given reactant (m/s);  $S_A$ =RH corrected aerosol surface area concentration ( $nm^2/cm^3$ );  $r$ =surface-weighted particle radius.

#### References:

- Li, X., Rohrer, F., Brauers, T., Hofzumahaus, A., Lu, K., Shao, M., Zhang, Y. H., and Wahner, A. (2014). Modeling of HCHO and CHOCHO at a semi-rural site in southern China during the PRIDE-PRD2006 campaign, *Atmospheric Chemistry and Physics*, 14, 12291-12305, 10.5194/acp-14-12291-2014.
- Riedel, T. P., Wolfe, G. M., Danas, K. T., Gilman, J. B., Kuster, W. C., Bon, D. M., Vlasenko, A., Li, S.-M., Williams, E. J., Lerner, B. M., Veres, P. R., Roberts, J. M., Holloway, J. S., Lefer, B., Brown, S. S., and Thornton, J. A. (2014). An MCM modeling study of nitryl chloride ( $ClNO_2$ ) impacts on oxidation, ozone production and nitrogen oxide partitioning in polluted continental outflow, *Atmos. Chem. Phys.*, 14, 3789–3800, <https://doi.org/10.5194/acp-14-3789-2014>.

---

Xue, L., Wang, T., Gao, J., Ding, A., Zhou, X., Blake, D. R., Fang, X., Saunders, S. M., Fan, S., Zuo, H., Zhang, Q., Wang, W. (2014). Ground-level ozone in four Chinese cities: precursors, regional transport and heterogeneous processes. *Atmospheric chemistry and physics*, 14(23), 13175-13188.

Wang, X., Chen, J., Cheng, T., Zhang, R., Wang, X. (2014) Particle number concentration, size distribution and chemical composition during haze and photochemical smog episodes in Shanghai[J]. *Journal of Environmental Sciences*, 26(009):1894-1902.

The other important issue is the HONO/NO<sub>2</sub> ratio which is set here to 2%, based on the Tan et al., 2019 paper. However that study examined Chinese megacities and I would expect HONO and NO<sub>2</sub> levels to be different in rural areas. I appreciate that without HONO measurements it is not possible to be very accurate on this point, but since the paper shows that HONO is a major source of OH, this issue should be discussed somewhere in the manuscript. I suggest at least a sensitivity study to assess how the estimate of HONO impacts the model results and hence the conclusions of the paper. If, on the other hand, the conditions in this study and in the Tan et al., 2019, paper are similar, that would bring into question the classification of the measurement site as "rural", which would necessarily reframe the subject and the conclusions of the paper.

Response: We agree that the HONO/NO<sub>2</sub> ratio in this study is different from that in Tan et al. (2019). To investigate the sensitivity of our results to the HONO/NO<sub>2</sub> ratio, a series of simulations with different HONO/NO<sub>2</sub> ratios were conducted and the results were summarized in Table 2. A lower HONO/NO<sub>2</sub> ratio (e.g. 0.005) could lead to decrease of OH radical by 15.3% and a higher ratio (e.g. 0.04) could increase OH concentration by

14.1%. This could be explained by the important role of HONO photolysis as one of the OH sources. Discussions on the sensitivity results have been added to the revised manuscript (Page 13, Line 258-266):

“Sensitive studies were conducted to quantify the influences of different HONO/NO<sub>2</sub> ratios on radical recycling (Text S3, Figure. S1 and Table S1). As expected, lower HONO/NO<sub>2</sub> ratio leads to lower HONO concentrations, and subsequent less OH generated from the photolysis of HONO. The sensitive study shows that when HONO/NO<sub>2</sub> ratio is 0.005, the daytime OH level could decrease by 15.3%. Vice versa, a higher HONO/NO<sub>2</sub> ratio (e.g., 0.04) can promote OH concentration by 14.08%. This result indicates that the photolysis of HONO is essential to the generation of OH, and therefore a simultaneous measurement of HONO is highly recommended for analyzing local radical recycling.”

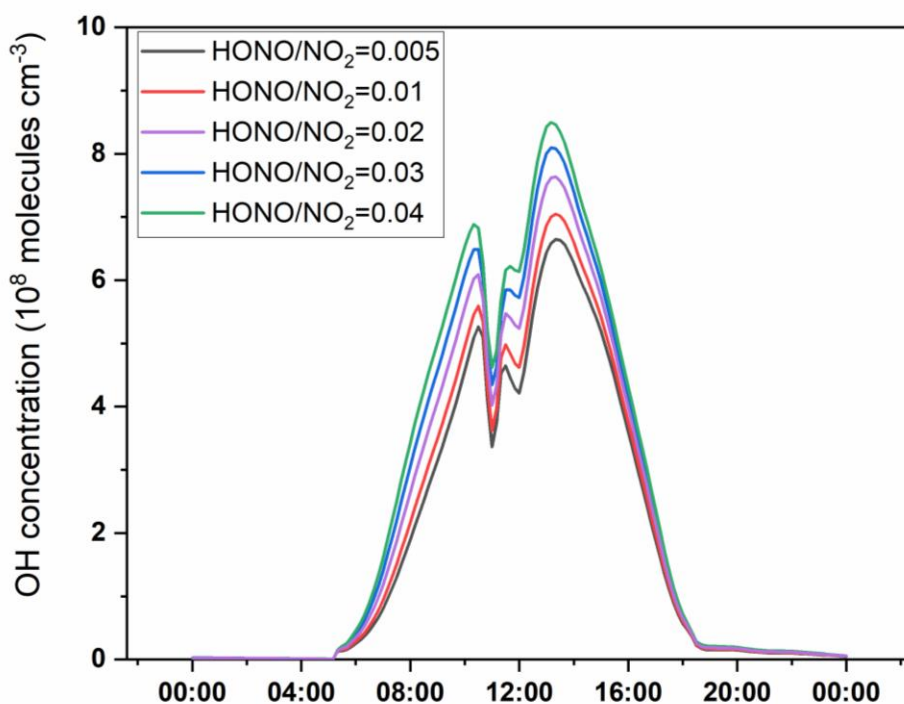


Fig. 1 Comparison of OH concentration under different HONO/NO<sub>2</sub> ratios.

---

**Table 2 Model sensitivity test result.**

HONO/NO <sub>2</sub> ratio	Change in OH (%)
0.005	-15.3%
0.01	-9.3%
0.03	7.5%
0.04	14.1%

With regards to the analysis of ozone and formaldehyde I am confused about the model setup. On line 141 it is said that O<sub>3</sub>, NO<sub>x</sub> and VOCs (does it include HCHO?) are constrained in the model. However, on lines 147-151 and in Figure S1, "simulated ozone" is discussed. It is also not clear if HCHO is constrained or not. A species can be either constrained or calculated (simulated) in a model, but not both. The larger point, however, is that if O<sub>3</sub> and/or HCHO are constrained, then the results in sections 3.4, 3.5, 3.6.2 and 3.6.3 need to be revised. It does not make much sense to look at the rate of production of a constrained variable because its value is set by the model and not calculated based on the values of the other variables. So the authors should first clarify whether O<sub>3</sub> and HCHO are constrained or calculated in the model and then amend the discussion in sections 3.4, 3.5, 3.6.2 and 3.6.3 accordingly.

Response: O<sub>3</sub> and HCHO were not constrained in our simulation, because we want to analyze the secondary formation of these compounds. To avoid misunderstanding, we have revised related descriptions in the revised manuscript (Line 146-147): " Hourly averaged concentrations of speciated VOCs (except HCHO), NO, NO<sub>2</sub> and meteorological parameters (such as T, RTH, P) were used to constrain the F0AM model."

---

Minor comments

In Table 1, and in the related text, I believe "42i" and "43i" need to be exchanged. Also, I suggest the detection limits and/or uncertainties are added to the Table 1.

Response: Thanks for the helpful advice. We have exchanged “42i” and “43i” in Table 1 and in the related text and add detection limits in Table 1.

line 103: correct to "Vaisala"

Response: We have corrected “Visala” into “Vaisala”

line 115: I imagine you mean 15m above the 5th floor?

Response: We are sorry for the unclear expression, and we mean the top of the 5-floor-high building is 15 m above the ground level. Therefore, we have revised this sentence into “The instruments were housed on the top of a 5-floor-high building, which was about 15 m above the ground level.”

line 142: correct to "RH".

Response: We have revised this word as suggested.

lines 143: correct to "nitrous acid".

Response: We have revised this word as suggested.

line 149: please define these indices (IOA, MB, NMB).

---

Response: The definition of IOA, MB and NMB are given in Line 153-157: “The index of agreement (IOA) , mean bias (MB) and normalized mean bias (NMB) are frequently used to estimate the model performance. These three parameters can be calculated by Equation (2) to (4), where  $S_i$ ,  $O_i$ , and  $\bar{O}$  are the simulated, observed, and average value of the target compound. “

$$IOA = 1 - \frac{\sum (S_i - O_i)^2}{\sum (|S_i - \bar{O}| + |O_i - \bar{O}|)^2} \quad (2)$$

$$MB = \frac{\sum (S_i - O_i)}{N} \quad (3)$$

$$NMB = \frac{\sum (S_i - O_i)}{\sum O_i} \times 100 \quad (4)$$

lines 199-201: I assume you are talking about simulated  $\text{NO}_3$  here. Please always make clear in the text, figures and captions, when you are talking about measurements and when about model results.

Response: Thanks for the reviewer’s valuable suggestion. We have specified the “simulated  $\text{NO}_3$ ” in Line 236-237. In addition, we have checked the similar unclear expression throughout the paper.

lines 205-207: I am not aware of  $\text{RO} + \text{NO}_3$  reactions forming  $\text{RO}_2$ . Can you please clarify and/or correct?

Response: We are sorry for this mistake. It should be the reaction of  $\text{VOCs} + \text{NO}_3$  that account for over 70%  $\text{RO}_2$  production during nighttime, and relevant description has been revised.

---

line 212: correct to "ozonolysis".

Response: We have corrected this error as suggested.



# Explicit modelling of isoprene chemical processing in polluted air masses in suburban areas of the Yangtze River Delta region: radical cycling and formation of ozone and formaldehyde

Kun Zhang <sup>a, b</sup>, Ling Huang <sup>a, b</sup>, Qing Li <sup>a, b</sup>, Juntao Huo <sup>c</sup>, Yusen Duan <sup>c</sup>, Yuhang Wang <sup>d</sup>, Yangjun Wang <sup>a, b</sup>, Qingyan Fu <sup>c</sup>, Li Li <sup>a, b\*</sup>

<sup>a</sup> School of Environmental and Chemical Engineering, Shanghai University, Shanghai, 200444, China

<sup>b</sup> Key Laboratory of Organic Compound Pollution Control Engineering, Shanghai University, Shanghai, 200444, China

<sup>c</sup> Shanghai Environmental Monitoring Center, Shanghai, 200235, China

<sup>d</sup> School of Earth and Atmospheric Sciences, Georgia Institute of Technology, Atlanta, GA, USA

*Correspondence to* Li Li (Lily@shu.edu.cn)

## Abstract

Ozone pollution has become one of the most severe environmental problems in China in recent years. Our online observations showed that high levels of O<sub>3</sub> were frequently observed in suburban areas of the Yangtze River Delta (YRD) region even there was no obvious ozone transport from the urban regions. To better understand the formation mechanism of local O<sub>3</sub> pollution and investigate the potential role of isoprene chemistry in the budgets of RO<sub>x</sub> (OH+HO<sub>2</sub>+RO<sub>2</sub>) radicals, synchronous observations of volatile organic compounds (VOCs), formaldehyde (HCHO) and meteorological parameters were conducted at a suburban site of the YRD region in 2018. Five episodes with elevated O<sub>3</sub> concentrations under stagnant meteorological conditions were identified; an observation-based model (OBM) with the Master Chemical Mechanism was applied to analyze the photochemical processes in these high-O<sub>3</sub>

---

episodes. High levels of O<sub>3</sub>, nitrogen oxides (NO<sub>x</sub>), and VOCs facilitated strong production and recycling of RO<sub>x</sub> radicals with the photolysis of oxygenated VOCs (OVOCs) being the primary source. Our results suggest that local biogenic isoprene is important to suburban photochemical processes. Removing isoprene could drastically slow down the efficiency of RO<sub>x</sub> recycling and reduce the concentrations of RO<sub>x</sub>. The absence of isoprene chemistry could further lead to decrease in the daily average concentration of O<sub>3</sub> and HCHO by 34% and 36%, respectively. This study underlines that the isoprene chemistry in suburban atmosphere becomes important with the participation of anthropogenic NO<sub>x</sub> and also provides insights into the radical chemistry that essentially drives the formation of secondary pollutants (e.g. O<sub>3</sub> and HCHO) in suburban YRD region.

**Keywords:** Isoprene; Observation-based model (OBM); Radical; Ozone; Yangtze River Delta

## 1. Introduction

The hydroxyl radical (OH), hydro peroxy radical (HO<sub>2</sub>) and organic peroxy radical (RO<sub>2</sub>), collectively known as RO<sub>x</sub> dominate the oxidative capacity of the atmosphere and hence govern the removal of primary contaminants (e.g. volatile organic compounds (VOCs)) and the formation of secondary pollutants (e.g. ozone (O<sub>3</sub>), secondary organic aerosols (SOAs)) (Liu et al., 2012;Xue et al., 2016). RO<sub>x</sub> radicals can undergo efficient recycling (e.g. OH→RO<sub>2</sub>→RO→HO<sub>2</sub>→OH) and produce O<sub>3</sub> and oxygenated VOCs (OVOCs) (Liu et al., 2012;Tan et al., 2019;Xue et al., 2016). In addition, the photolysis of OVOCs can in turn produce primary RO<sub>2</sub> and HO<sub>2</sub> radicals, and further accelerate the recycling of RO<sub>x</sub> (Liu et al., 2012). The reaction rates of different VOCs with RO<sub>x</sub> vary significantly (Atkinson and Arey, 2003; Atkinson et al., 2006). For instance, the reaction rate constants for OH with ethane and ethene are  $0.248 \times 10^{-12}$  (cm molecule<sup>-1</sup> s<sup>-1</sup>) and  $8.52 \times 10^{-12}$  (cm molecule<sup>-1</sup> s<sup>-1</sup>), respectively. Among the hundreds thousands of VOC species, isoprene (C<sub>5</sub>H<sub>8</sub>, 2-methyl-1,3-butadiene) is one of the

---

most active species, and also the most abundant biogenic VOCs (BVOCs) species globally (Wennberg et al., 2018). Isoprene emissions from biogenic sources have been extensively studied over past decades (Gong et al., 2018) and recent works have switched from emissions to the degradation pathways and the impact of isoprene chemistry on regional forest chemistry (Gong et al., 2018; Wolfe et al., 2016a). Previous studies showed that isoprene could be quickly oxidized by atmospheric oxidants (e.g. OH, O<sub>3</sub> or NO<sub>3</sub>) (Wolfe et al., 2016a; Gong et al., 2018; Jenkin et al., 2015). Due to the rapid reaction between OH and isoprene ( $100 \times 10^{-12} \text{ cm}^3 \text{ molecule}^{-1} \text{ s}^{-1}$  at 298 K), more than 90% of the total daytime isoprene is removed via this reaction (Wennberg et al., 2018). The reaction between OH and isoprene is initiated by the addition of OH and can generate isoprene hydroxyp peroxy radicals (ISOPO<sub>2</sub>) (Wennberg et al., 2018; D'Ambro et al., 2017; Liu et al., 2013; Jenkin et al., 2015). ISOPO<sub>2</sub> isomers could then interconvert rapidly due to reversible O<sub>2</sub> addition and are finally removed via reactions with HO<sub>2</sub> or NO (Jenkin et al., 2015; Wolfe et al., 2016a). Hence, the degradation process of isoprene is tightly associated with RO<sub>x</sub> recycling. According to He et al. (2019), isoprene chemistry could strongly influence the photochemical formation of O<sub>3</sub>, with a relative incremental reactivity (RIR) of ~0.06%/%. In addition to O<sub>3</sub>, HCHO is formed via several pathways during the depletion of isoprene (Jenkin et al., 2015; Wolfe et al., 2016a) and HCHO formation is found to be highly sensitive to isoprene (Zeng et al., 2019).

The Yangtze River Delta (YRD) region is one of the most developed city-clusters in eastern China and has been suffering from serious O<sub>3</sub> pollution (Zhang et al., 2019; Zhang et al., 2020a; Chan et al., 2017). At the suburban area of YRD, high levels of O<sub>3</sub> were frequently observed (Zhang et al., 2019; Zhang et al., 2020a). A number of studies have been conducted to investigate the relationships between O<sub>3</sub> precursors and O<sub>3</sub> (Chan et al., 2017; Lin et al., 2020; Zhang et al., 2020a; Zhang et al., 2020b), but few have attempted to address the atmospheric oxidizing capacity and radical chemistry involved in these complicated

---

photochemical processes (Tan et al., 2019;Zhu et al., 2020b). Previous studies have pointed out that high levels of O<sub>3</sub> at suburban areas of Shanghai could be attributed to the transport of O<sub>3</sub> or O<sub>3</sub> precursors from urban areas (Lin et al., 2020; Zhang et al., 2019). However, high O<sub>3</sub> concentrations were frequently observed in suburban areas under stable meteorological conditions. Given the high vegetation coverage in suburban YRD and weak transport of air masses, the importance of local isoprene chemistry to ozone formation remains unclear.

In this study, we conducted a comprehensive set of in-situ observations of isoprene, meteorological parameters, and trace gases to understand the important impact of isoprene chemistry on atmospheric photochemical processes in suburban YRD region. An observation-based model (OBM) was used to explore the role of local isoprene chemistry in radical budgets and the formation of O<sub>3</sub> and HCHO. Results from this study can provide insights into the isoprene chemistry in the suburban region of a fast-developing city-cluster.

## 2. Methodology

### 2.1 Measurement site and techniques

The observations were conducted at a supersite (120.98°E, 31.09°N) in the suburban areas of the YRD region (Figure 1). It is located in the west of Shanghai and is close to the Dianshan Lake Scenic area, which has high vegetation coverage. To investigate the local isoprene chemistry and its influence on O<sub>3</sub> and HCHO formation, continuous measurements were conducted from Apr. 7 to Sep. 25, 2018, when the photochemical reactions are active and ozone formation is significant.

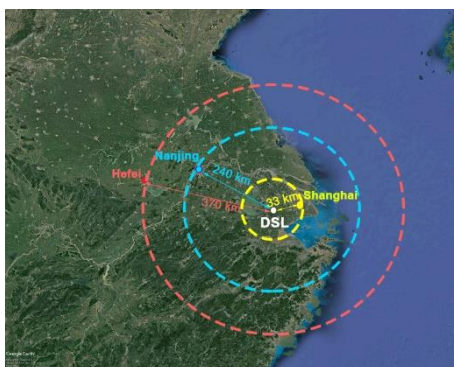


**Figure 1.** Location of the Dianshan lake supersite (white dot) in the **suburban** areas of YRD region.

This picture was created with Google Earth© on 23<sup>rd</sup> July 2020.

**Table 1.** Measurements performed during the ozone season

Species/Parameter	Experimental Technique	Time resolution	Lower Detectable limit
O <sub>3</sub>	Model 49i, Thermo Fischer Scientific, USA	60 s	0.5 ppbv
NO and NO <sub>2</sub>	Model 42i, Thermo Fischer Scientific, USA	60 s	0.4 ppbv
CO	Model 48i, Thermo Fischer Scientific, USA	60 s	40 ppbv
HCHO	AL4021, Aero-Laser, GER	90 s	0.1 ppbv
VOCs species	GC866, Agilent., USA	1 hour	-
Temperature, relative humidity, wind speed and wind direction	Meteorological station, Vaisala, NLD	60 s	-

The **measuring instruments** are shown in Table 1. Wind speed (WS), wind direction (WD), temperature (T), and relative humidity (RH) were simultaneously observed by a meteorological station (**Vaisala**., FIN). According to China's air quality standard, several criteria air pollutants were measured during this experiment. O<sub>3</sub> was measured by an ultraviolet photometric analyzer (Model 49i, Thermo Fischer Scientific., USA), which has a detection limit of **0.5** ppbv at **60 second** resolution. 1 min resolution of nitrogen oxides (NO and NO<sub>2</sub>) data were simultaneously observed by a chemiluminescence instrument (Model **42i**, Thermo Fischer Scientific., USA), which has a detection limit of **0.4** ppbv. Carbon monoxide was monitored by a gas filter correlation infrared absorption analyzer (Model 48i, Thermo Fischer Scientific., USA), which has a detection limit of 0.04 ppm. All the online instruments used for gas analyzer were auto-zero every day, and were multi-point calibrated every month. All the instruments used for the

---

online observation were housed on top of a 5-floor-high building, which was about 15 m above the ground level.

A total of 55 VOC species, including 28 alkanes, 10 alkenes, 16 aromatics and acetylene were continuously analyzed at our sampling site by two online gas chromatograph with flame ionization detector (GC-FID) systems (GC-866 airmoVOC C<sub>2</sub>-C<sub>6</sub> #58850712 and airmoVOC C<sub>6</sub>-C<sub>12</sub> #283607112, Agilent., USA) with a time resolution of 1 hour during our experiment. Ambient samples are directly inhaled into this system by a pump. Low carbon VOCs (C<sub>2</sub>-C<sub>6</sub>) are captured by a low temperature (-10 °C) preconcentration system, while high carbon VOCs are concentrated by a built-in room temperature preconcentration system. Then the preconcentration systems are heated and desorb VOCs, which are then carried into chromatographic columns by helium. Individual VOCs separated in the columns are eventually detected by FID systems. Formaldehyde (HCHO) was continuously measured by a Hantzsch fluorescence technique (AL4201, Aerolaser GmbH., GER), which is based on fluorometric Hantzsch reaction in the liquid phase, requiring the quantitative transfer of HCHO from gas phase to liquid phase. A Hantzsch reagent (acetylacetone) was used in this instrument.

## 2.2 Observation-based model

A user-friendly zero-dimensional (0-D) box model (F0AM) was used to simulate the chemical processes in the atmosphere in this study. This model was developed by Wolfe et al.(2016b) based on University of Washington Chemical Model (UWCM). Dry deposition, aloft exchange, and atmospheric dilution were considered in this model. We chose the Master Chemical Mechanism (MCM) v3.3.1 as the chemical mechanism with more than 5,800 chemical species and 17,000 reactions, which enables a detailed description of the complex reactions. In addition to gas-phase reactions, several heterogenous processes including the uptake of HO<sub>2</sub>, N<sub>2</sub>O<sub>5</sub> and HCHO on aerosol surface, and heterogenous source of HONO were also considered in our simulation. These reactions rate constants and uptake coefficient were

obtained from the study of Riedel et al. (2014), Xue et al. (2014) and Li et al. (2014). Since key parameters such as aerosol surface areas ( $S_A$ ) and particle diameters ( $r$ ) were not measured during our observation, an average  $S_A$  ( $640 \text{ nm}^2/\text{cm}^3$ ) was obtained from the field campaign in Shanghai (Wang et al., (2014)).

**Table 2. Heterogeneous reactions and associated rate constants used in the OBM model**

Reactions	Reaction rate constant	Reference
$N_2O_5 \rightarrow CLNO_2 + HNO_3$	$\gamma\omega S_A/4$ (for $CLNO_2$ formation) $(2 - \phi)\gamma\omega S_A/4$ (for $HNO_3$ formation)	Riedel et al. (2014)
$NO_2 \rightarrow HONO$	$k_g = \frac{1}{8} \times \omega\gamma_g \left(\frac{S}{V}\right)$ $k_a = \frac{1}{4} \omega\gamma_a S_A$	Xue et al. (2014)
$HO_2 \rightarrow \text{products}$	$k = \left(\frac{r}{D_g + \gamma} \omega\right)^{-1} S_A$	Xue et al. (2014)
$HCHO \rightarrow \text{products}$	$k = \frac{1}{4} \omega\gamma S_A$	Li et al. (2014)

$\gamma$ = uptake coefficient for the given reactant with aerosol surface area;  $\phi$  = product yield;  $\omega$ =mean molecular speed of the given reactant (m/s);  $S_A$ =RH corrected aerosol surface area concentration ( $\text{nm}^2/\text{cm}^3$ );  $r$ =surface-weighted particle radius.

Photolysis frequencies ( $J$  values) were calculated by a trigonometric parameterization based on solar zenith angle (SZA):

$$J = I \cos(SZA)^m \exp(-n \sec(SZA)) \quad (1)$$

where  $I$ ,  $m$  and  $n$  are constants unique to each photolysis reaction, derived from least-squares fits to  $J$  values computed with fixed solar spectra and literature cross-section and quantum yields (Wolfe et al., 2016b). Hourly averaged concentrations of speciated VOCs (except  $HCHO$ ),  $NO$ ,  $NO_2$ ,  $CO$  and meteorological parameters (such as  $T$ ,  $RH$  and  $P$ ) were used to constrain the F0AM model. Nitrous acid ( $HONO$ ) was not measured during our observation.

Therefore, it was fixed as 2% of the observed NO<sub>2</sub> concentration. This constant ratio is well observed in different field studies and performed well in previous box model studies (Tan et al., 2019). Before each simulation, the model will run 3 days as spin up to reach a steady state for unmeasured species (e.g., OH and NO<sub>3</sub> radicals). The comparison of simulated and observed O<sub>3</sub> and HCHO concentrations is shown in Figure S1 and Figure S2. The index of agreement (IOA), mean bias (MB) and normalized mean bias (NMB) are frequently used to estimate the model performance. These three parameters can be calculated by Equation (2) to (4), where S<sub>i</sub>, O<sub>i</sub>, and  $\bar{O}$  are the simulated, observed, and average observed value of the target compound. In this study, the IOA, MB and NMB of O<sub>3</sub> was 0.90, 0.76 and 10%, respectively. This result suggests that the model can reasonably reproduce the variations of O<sub>3</sub> and could be used for further analysis. As for HCHO, the IOA, MB, and NMB was 0.74, 2.43 and 48%, respectively. In general, the model overestimated HCHO concentration, especially on July 29 and July 30. According to previous studies, the inconsistency between simulated and observed HCHO could be caused by the uncertainties in the treatment of dry deposition, faster vertical transport, uptake of HCHO, and fresh emissions of VOCs precursors (Li et al., 2014). But the result still provides valuable information of secondary formation of HCHO at suburban area. To quantify the atmospheric oxidative capacity (AOC) changes in response to isoprene chemistry, two parallel scenarios (S0 and S1) were conducted with isoprene chemistry disabled in S1. In both cases, identical chemical mechanism and meteorological conditions were used to drive model simulations. Through a comparative analysis of the scenarios, the impact of isoprene chemistry on AOC and secondary formation of O<sub>3</sub> and HCHO can be obtained.

$$IOA = 1 - \frac{\sum (S_i - O_i)^2}{\sum (|S_i - \bar{O}| + |O_i - \bar{O}|)^2} \quad (2)$$

$$MB = \frac{\sum (S_i - O_i)}{N} \quad (3)$$



$$NMB = \frac{\sum(s_i - o_i)}{\sum o_i} \times 100\% \quad (4)$$

### 3. Results and discussions

#### 3.1 Overview of the observations

To investigate the impact of local chemistry on ozone formation, five days with low daily average wind speed (<2m/s) and high maximum daily 8-h average (MDA8) O<sub>3</sub> concentration (>74.7 ppb) were identified as typical local chemistry cases. Figure 2 shows the time series of observed meteorological parameters (P, T, and RH), trace gases (NO, NO<sub>2</sub> and O<sub>3</sub>), isoprene and HCHO on selected days. During those episodes, the air masses reaching the site were mainly from southeast and southwest (Figure 2). The weak wind was not conducive to the regional transportation of air pollutants. The observed O<sub>3</sub>, NO<sub>2</sub>, NO, CO, and TVOC ranged from 1.40 to 155.40 ppbv (52.72 ± 44.43 ppbv, average value, the same below), 5.36 to 57.95 ppbv (21.58 ± 12.88 ppbv), 0.75 to 54.51 ppbv (5.40 ± 8.13 ppbv), 400 to 960 ppbv (597 ± 153 ppbv), and 2.34 to 20.33 ppbv (7.28 ± 4.32 ppbv) respectively. During the five episodes, the average concentrations of alkanes, alkenes, and aromatics were 13.97 ± 9.12, 3.27 ± 2.31, and 4.93 ± 2.69 ppbv, which were about 53%, 18%, and 50% higher than of the whole observation. The conditional probability function (CPF) is applied to exhibit the relationship between high O<sub>3</sub> concentrations and wind (Figure 3). The detailed description of CPF can be found in supplemental information (Text S1). The result suggests that high O<sub>3</sub> concentrations (>131 ppb) was usually observed when the site was influenced by weak south wind. This implies that high O<sub>3</sub> was most likely formed locally. Although this site is far away from urban areas, high levels of NO were found during early morning, which is likely caused by nearby fresh emissions. As for NO<sub>2</sub>, only one peak was found at dusk. This was different from the results in urban areas (Zhang et al., 2019). It is worth noting that NO<sub>2</sub> and O<sub>3</sub> concentrations were high even during nighttime, suggesting that the AOC remained high at nighttime. The daily average isoprene concentrations were 0.37 ± 0.36 ppbv, which is comparable to that observed by Gong et al.

(2018) at a forested mountaintop site ( $0.287 \pm 0.032$  ppbv). To roughly estimate the influence of isoprene on atmospheric oxidation capability, we adopted the approach given in the study of Zhu et al. (2020a) to calculate the OH reactivity ( $k_{OH}$ ). The result suggested that isoprene, accounting for ~19% of the total  $k_{OH}$ , was the most significant VOC specie from the perspective of  $k_{OH}$ , with an average value of  $0.89 \pm 0.44$  s<sup>-1</sup>. This indicates the significant role of isoprene in the photochemistry in suburban area. The average HCHO was  $5.01 \pm 3.80$  ppbv, which was ~2 times of that observed at a rural site of Hong Kong (Yang et al., 2020). It is worth noting that HCHO could reach 18.69 ppbv at midday. Based on the explicit calculation, the total concentration of OVOC was obtained. Due to the complexity of OVOC formation, which could have hundreds of precursors for just one OVOC specie, and the complicated chain reactions converting VOCs to OVOCs, it is difficult to give the accurate relationship between VOCs to OVOCs. Since VOCs were mainly oxidized by OH and O<sub>3</sub> during daytime, in this study, we chose multi-linear regression model (given in Eq.(5) ) to explore the roughly relationship between VOCs and simulated OVOCs.

$$[OVOC] = \beta_0 + \beta_1[Alkane] + \beta_2[Alkene] + \beta_3[Aromatic] + \beta_4[OH] + \beta_5[O_3] \quad (5)$$

where  $\beta_0, \beta_1, \beta_2, \beta_3, \beta_4$ , and  $\beta_5$  are the coefficient from linear regression; [OVOC] and [OH] are the simulated concentration of OVOC and OH, respectively; [Alkane], [Alkene], [Aromatic], [O<sub>3</sub>] are the observed concentration of alkanes, alkenes, aromatics, and O<sub>3</sub>, respectively. The Sig value and statistical reliability criteria (R) was 0.000 and 0.853 (shown in Table S2), respectively, indicating that the linear relationship represented by equations (5) is statistically reliable. The  $\beta_1, \beta_2, \beta_3$  was 0.027, 0.623, and 0.820, respectively, suggesting that alkenes and aromatics are significant for the simulated OVOC concentration.

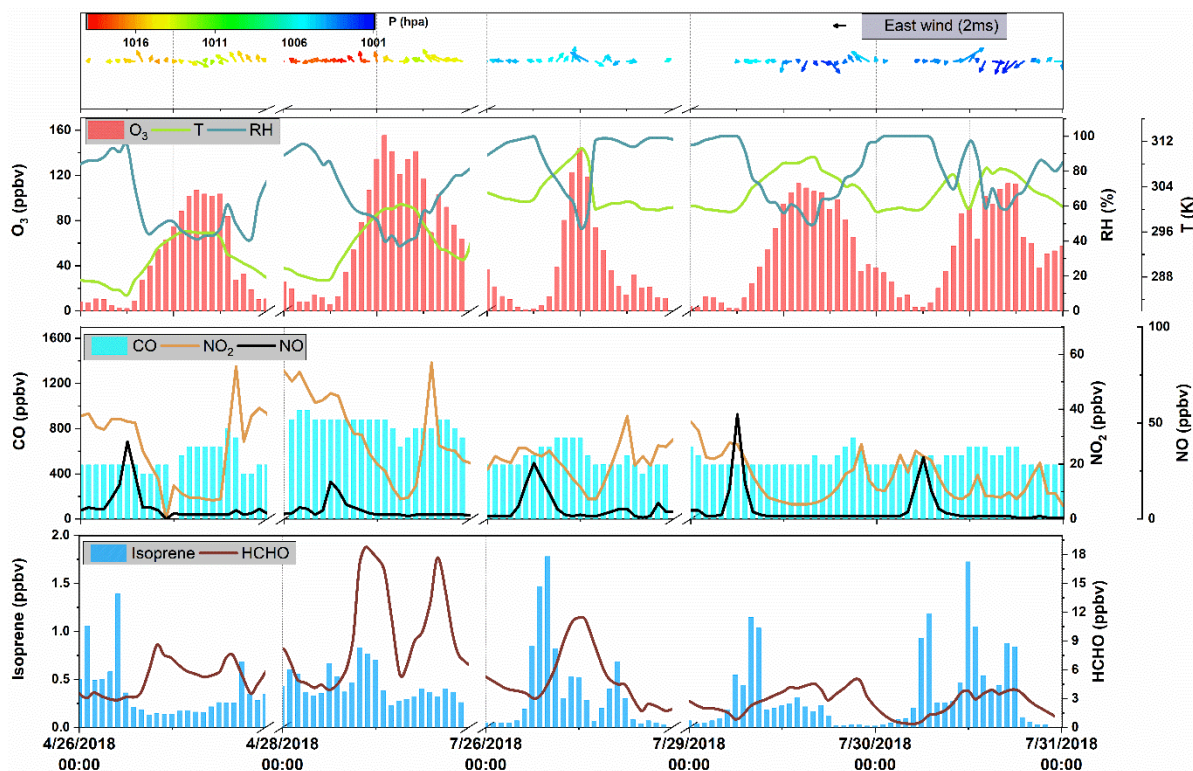
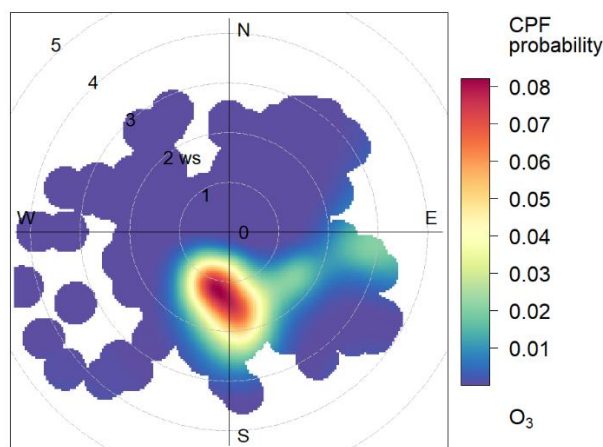


Figure 2. Time series of hourly averages for trace gases, isoprene, HCHO, and meteorological parameters.



CPF at the 95th percentile (=131)

Figure 3. CPF polar plot of O<sub>3</sub> at DSL station.

### 3.2 Simulated concentrations of radicals

Figure 4 shows the simulated average diurnal variation of major radicals in the base scenario (S0). The average concentrations of OH, HO<sub>2</sub>, RO<sub>2</sub>, and NO<sub>3</sub> were estimated at  $2.11 \times 10^6$ ,  $1.04 \times 10^8$ ,  $0.90 \times 10^9$ , and  $3.49 \times 10^8$  molecules cm<sup>-3</sup>, respectively. The simulated daily

---

average OH concentration lies between the simulated values during the summer in Beijing ( $9 \times 10^6$  molecules  $\text{cm}^{-3}$ ) and the simulated value at a suburban site in Hong Kong in 2013 ( $1.5 \pm 0.2 \times 10^6$  molecules  $\text{cm}^{-3}$ ) (Liu et al., 2019; Xue et al., 2016). In addition, the average simulated daytime OH concentration was ~50% lower than that simulated at a forested mountaintop site in southern China (Gong et al., 2018). To verify the performance of OBM model, regional mixing ratios of OH during daytime were also calculated by a parameterization method using measured ethylbenzene and *m,p*-xylene ratios (see Text S2). The calculated average regional concentrations of OH ( $8.39 \pm 5.11 \times 10^6$  molecules  $\text{cm}^{-3}$ ) was in the same magnitude of the OBM-simulated result ( $4.59 \pm 5.11 \times 10^6$  molecules  $\text{cm}^{-3}$ ), suggesting that the OBM-simulated radical concentration is reliable. The maximum HO<sub>2</sub> concentration simulated for DSL site ( $6.19 \times 10^8$  molecules  $\text{cm}^{-3}$ ) was close to that reported in Beijing ( $6.8 \times 10^8$  molecules  $\text{cm}^{-3}$ ) (Liu et al., 2012), but was ~32% higher than that in Wuhan ( $4.7 \times 10^8$  molecules  $\text{cm}^{-3}$ ) (Zhu et al., 2020a). Pretty high levels of simulated NO<sub>3</sub> (as high as  $\sim 19 \times 10^8$  molecules  $\text{cm}^{-3}$ ) was found during nighttime. The average simulated nocturnal NO<sub>3</sub> concentration was  $8.80 \times 10^8$  molecule  $\text{cm}^{-3}$ , which was ~47% higher than that simulated in the study of Gong et al. (2018). As aforementioned, during nighttime, pretty high levels of NO<sub>2</sub> (27.71 ppbv) and O<sub>3</sub> (30.05 ppbv) was observed, which favored the formation of NO<sub>3</sub>. Interestingly, a high level of RO<sub>2</sub> was also found during nighttime. This result is different from the study of Liu et al. (2012), which found the maximum value of RO<sub>2</sub> during daytime. By separating the formation pathways of RO<sub>2</sub>, we found that during nighttime, over 70% RO<sub>2</sub> was produced via the oxidation of VOCs by NO<sub>3</sub> radical, suggesting that the nighttime chemistry in the suburban site was also very important.

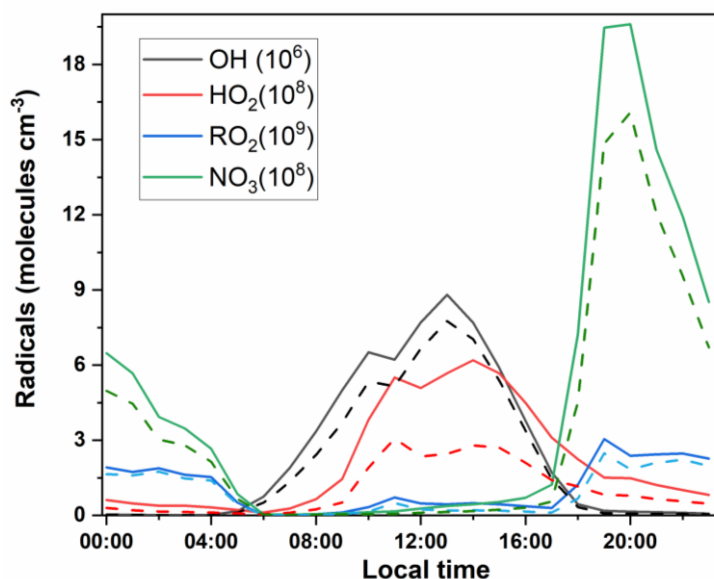


Figure 4. Simulated average diurnal variation of OH, HO<sub>2</sub>, RO<sub>2</sub> and NO<sub>3</sub> in S0 (solid lines) and S1 (dash lines).

### 3.3 Recycling of RO<sub>x</sub> radicals

Figure 5(A) shows the primary sources of RO<sub>x</sub> in S0 and the detailed daytime budget of RO<sub>x</sub>. Minor RO<sub>x</sub> sources, e.g. ozonolysis of alkenes, are not shown. The photolysis of O<sub>3</sub> was the predominant primary source of OH, with a daytime mean production rate of 0.50 ppbv h<sup>-1</sup>, which was comparable to that found by Liu et al. (2012) in Beijing, but was 0.40 ppbv h<sup>-1</sup> lower than the result in the study of Xue et al. (2016). Another important OH source is the photolysis of HONO, contributing 0.32 ppbv h<sup>-1</sup> of daytime OH production in our simulation. This value is much lower than the results of Liu et al. (2019) and Xue et al. (2016). Such low value was most likely caused by the excessive constrain on HONO since HONO was not directly monitored during our experiment. Sensitive studies were conducted to quantify the influence different of HONO/NO<sub>2</sub> ratio on radical recycling (Text S3, Figure. S1 and Table S1). As expected, a lower HONO/NO<sub>2</sub> ratio leads to a lower HONO concentration, and subsequent less OH reduce generated from the photolysis of HONO. The sensitive studies show that when HONO/NO<sub>2</sub> ratio is 0.005, the daytime OH level could decrease by 15.28%. Vice versa, a higher HONO/NO<sub>2</sub> (e.g., 0.04) can promote OH concentration by 14.08%. This result indicates

---

that the photolysis of HONO is essential to the generation of OH, and therefore a simultaneous measurement of HONO is highly recommended for the analysis of local radical recycling in the future. As for HO<sub>2</sub>, the photolysis of OVOC (excluding HCHO) is the predominant source with a daytime mean production rate of 0.65 ppbv h<sup>-1</sup> and maximum reaching 0.92 ppbv h<sup>-1</sup>, which is comparable to Xue et al. (2016). The photolysis of HCHO can also contribute 0.48 ppbv h<sup>-1</sup> to the daytime production of HO<sub>2</sub>, which is close to the results of Xue et al. (2016). As for RO<sub>2</sub>, the photolysis of OVOC was the largest source (0.57 ppbv h<sup>-1</sup>), which was relatively lower than the results found at urban site (Liu et al., 2012). From the RO<sub>x</sub> perspective, the daytime primary radical production in DSL site was dominated by the photolysis of OVOC (except for HCHO), followed by the photolysis of HCHO and O<sub>3</sub>. But the photolysis of HONO can become the overriding RO<sub>x</sub> source around run rising, which suggests that HONO can be an important OH reservoir species during nighttime. Summing up all the sources of RO<sub>x</sub> gives a total primary daytime RO<sub>x</sub> production rate of 2.55 ppbv h<sup>-1</sup> (0.84 ppbv h<sup>-1</sup> for OH, 1.14 ppbv h<sup>-1</sup> for HO<sub>2</sub>, and 0.57 ppbv h<sup>-1</sup> for RO<sub>2</sub>), which was 61~69% lower than those in Beijing (6.6 ppbv h<sup>-1</sup>, Liu et al. (2012)) and Hong Kong (8.11 ppbv h<sup>-1</sup>, Xue et al. (2016)), indicating that the recycling of RO<sub>x</sub> in Beijing and Hong Kong could be much reactive.

RO<sub>x</sub> radicals are ultimately removed from the atmosphere via deposition of radical reservoir species, e.g. H<sub>2</sub>O<sub>2</sub>, HNO<sub>3</sub>, and ROOH (Liu et al., 2012). The terminate processes of RO<sub>x</sub> was dominated by their reactions with NO<sub>x</sub>. Specifically, the reaction of OH+NO<sub>2</sub>, RO<sub>2</sub>+NO<sub>2</sub>, RO<sub>2</sub>+NO, forming HNO<sub>3</sub>, RO<sub>2</sub>NO<sub>2</sub>, and RONO<sub>2</sub>, accounting for 2.42, 0.56, and 0.41 ppbv h<sup>-1</sup> of the RO<sub>x</sub> radical sink during daytime. This is consistent with the understanding that reactions with NO<sub>x</sub> usually dominate the radical sink in high NO<sub>x</sub> environments (Xue et al., 2016; Liu et al., 2012). In addition, RONO<sub>2</sub> and RO<sub>2</sub>NO<sub>2</sub> could in turn react with OH, leading to 0.41 ppbv h<sup>-1</sup> of daytime OH sinks (Figure 6). Summing up the primary sources and sinks gives a

negative value of net RO<sub>x</sub> production, suggesting that the RO<sub>x</sub> was in a stage of gradual depletion.

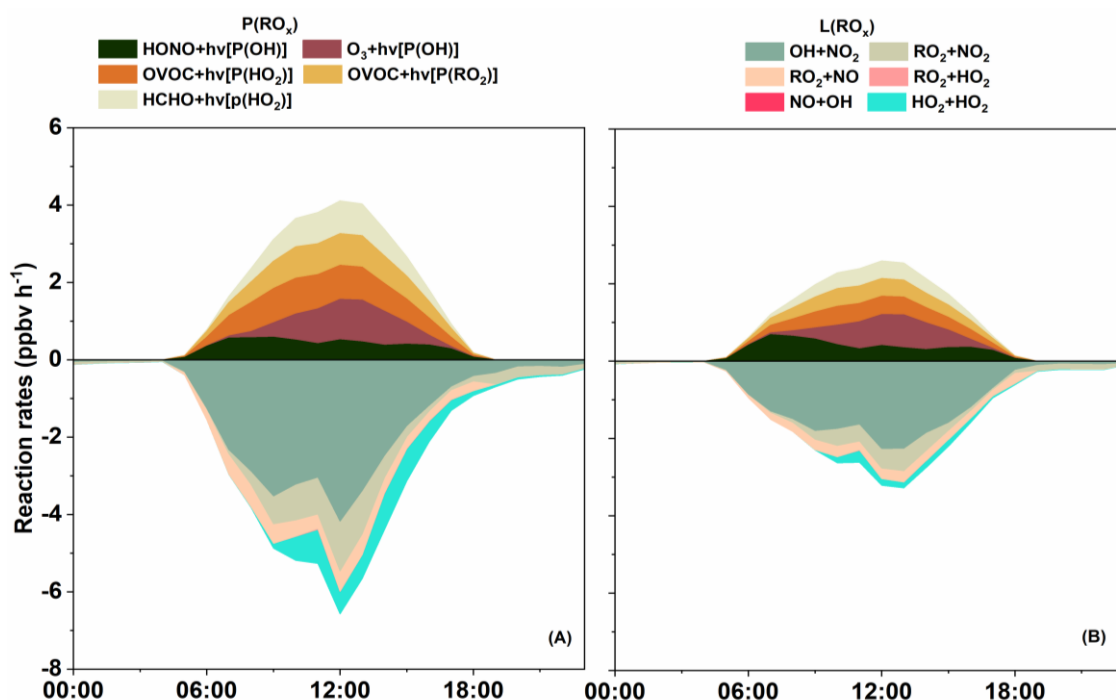


Figure 5. Simulated primary daytime sources and sink of RO<sub>x</sub> in S0 (A) and S1 (B).

The daytime (6:00-18:00) average budget of RO<sub>x</sub> is shown in Figure 6, with primary sources of RO<sub>x</sub> in red, sinks of RO<sub>x</sub> in blue, and recycling processes in black. In the recycling of RO<sub>x</sub>, the production of OH was dominated by the reaction of HO<sub>2</sub>+NO (8.29 ppbv h<sup>-1</sup>). As for RO<sub>2</sub>, it was produced by the reaction of OH with OVOC (3.02 ppbv h<sup>-1</sup>), alkyl (RH) (1.21 ppbv h<sup>-1</sup>), and peroxides (0.14 ppbv h<sup>-1</sup>). The reaction of RO<sub>2</sub>+NO can result in strong production of RO (3.87 ppbv h<sup>-1</sup>). The reaction of RO and O<sub>2</sub> was the major contributor to HO<sub>2</sub> production, followed by the reaction of OH with CO (1.89 ppbv h<sup>-1</sup>), OVOC (1.59 ppbv h<sup>-1</sup>), and RH (0.15 ppbv h<sup>-1</sup>). It should be noted that the top two fast reactions within the recycling of RO<sub>x</sub> (HO<sub>2</sub>+NO and RO<sub>2</sub>+NO) were related to NO<sub>x</sub>. As mentioned in the study of Liu et al. (2012), this result could be mainly due to the abundance of NO (e.g. ~50 ppbv in the morning). Obviously, these recycling processes dominate the total production of OH, HO<sub>2</sub> and RO<sub>2</sub> radicals. As suggested in the study of Xue et al. (2016) and Liu et al. (2012), the



radical propagation is efficient and enhances the effect of the newly produced radicals in the polluted atmospheres with the co-existence of abundant NO<sub>x</sub> and VOCs.

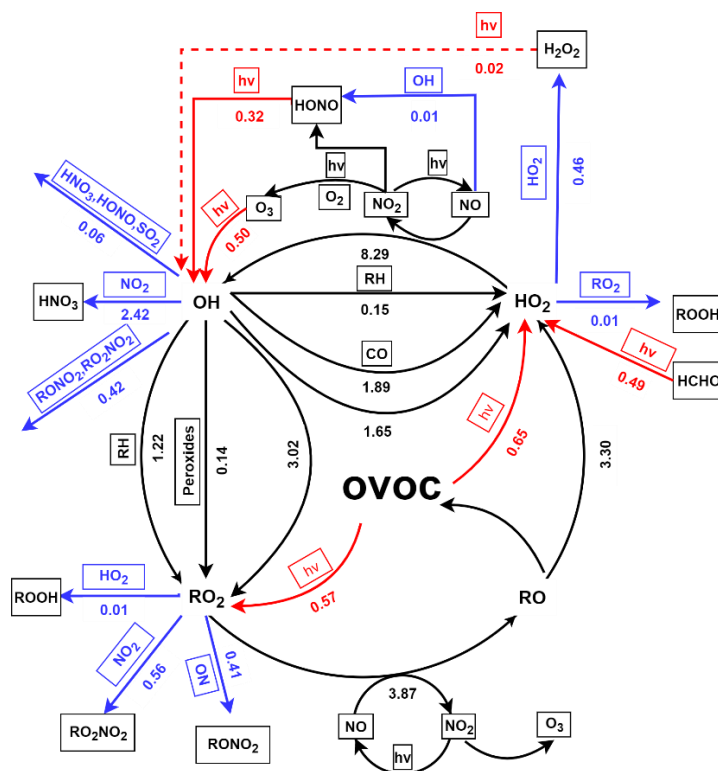


Figure 6. Summary of daytime (06:00-18:00) average budgets of RO<sub>x</sub> radicals (in ppbv h<sup>-1</sup>).

Primary RO<sub>x</sub> sources and sinks are in red and blue, respectively, and the black lines represent the processes in RO<sub>x</sub> and NO<sub>x</sub> recycling.

### 3.4 Formation and sink of O<sub>3</sub>

Figure 7 illustrates the diurnal variation of simulated O<sub>3</sub> formation and sink pathways in S0. Also shown is the simulated average diurnal pattern of O<sub>3</sub> concentration and the net O<sub>3</sub> production rate. In the troposphere, the formation of O<sub>3</sub> is via the reactions of NO with peroxy radicals (e.g. HO<sub>2</sub> and RO<sub>2</sub>) (Liu et al., 2012; Xue et al., 2016; Zhu et al., 2020a). On average, the reaction of HO<sub>2</sub>+NO and RO<sub>2</sub>+NO attributed 5.05 and 4.62 ppbv h<sup>-1</sup> of the production of O<sub>3</sub>. The maximum rate of HO<sub>2</sub>+NO (15.36 ppbv h<sup>-1</sup>) and RO<sub>2</sub>+NO (13.26 ppbv h<sup>-1</sup>) both occurred at 13:00. The total daytime production rate of O<sub>3</sub> (P(O<sub>3</sub>)) is the sum of HO<sub>2</sub>+NO and RO<sub>2</sub>+NO at 17.86 ppbv h<sup>-1</sup>, which lies between that simulated in Beijing (32 ppbv h<sup>-1</sup>, Liu et al. (2012)) and Hong Kong (6.7 ppbv h<sup>-1</sup>, Liu et al. (2019)). Due to the fast cycling of both O<sub>3</sub>



and NO<sub>2</sub>, the sink of O<sub>3</sub> was due to several reactions leading to the destruction of O<sub>3</sub> and NO<sub>2</sub>. In our cases, the reaction of NO<sub>2</sub>+OH becomes the predominant scavenging pathways of O<sub>3</sub>, with an average daytime reaction rate of 1.89 ppbv h<sup>-1</sup> (49%, percentage of the total O<sub>3</sub> sink rate, same below). This is comparable to the study of Liu et al. (2012 and 2019). The reaction of RO<sub>2</sub>+NO<sub>2</sub> was the second contributor to O<sub>3</sub> sink, with a mean contribution of 0.62 ppbv h<sup>-1</sup> (16%). Other pathways, e.g. photolysis of O<sub>3</sub>, ozonolysis of alkenes, and O<sub>3</sub>+HO<sub>2</sub>, together contributed 1.11 ppbv h<sup>-1</sup> of the total sink rate of O<sub>3</sub> during daytime. The daytime mean L(O<sub>3</sub>) was 3.87 ppbv h<sup>-1</sup>, which was ~22% of P(O<sub>3</sub>), suggesting that O<sub>3</sub> could efficiently accumulate during daytime. The net production of O<sub>3</sub> (P(O<sub>3</sub>)-L(O<sub>3</sub>)) is also shown in Figure 7. The maximum O<sub>3</sub> concentration was found at around 16:00, which was also observed in other suburban sites (Zong et al., 2018; Zhang et al., 2019). It is worth noting that, the reaction of alkenes+O<sub>3</sub>/NO<sub>3</sub> serves as an important pathway of O<sub>3</sub> sink during nighttime (as high as 2.30 ppbv h<sup>-1</sup>).

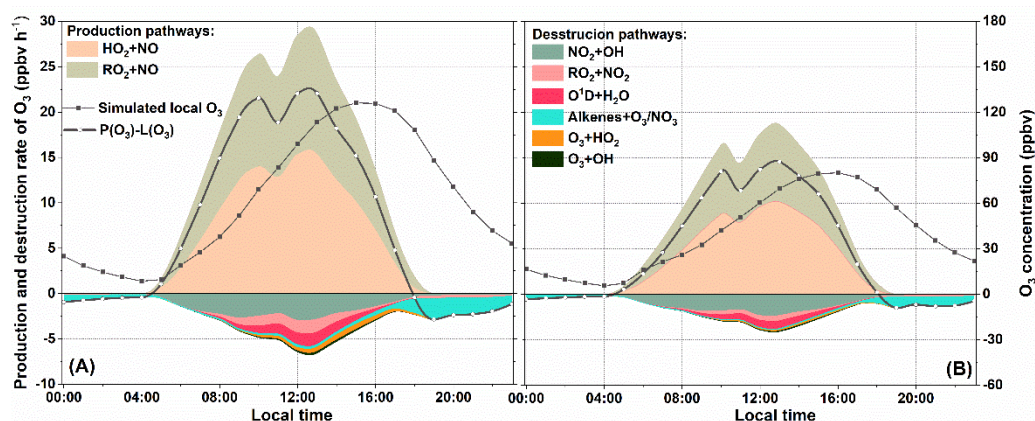


Figure 7. Simulated average diurnal profiles of O<sub>3</sub> formation and sink rates (ppbv h<sup>-1</sup>) in S0 (A) and S1 (B).

### 3.5 Formation and sink of HCHO

As aforementioned, high levels of HCHO was observed at DSL. Figure 8 (A) shows the production and sink pathways of HCHO in S0. On average, HCHO formation was dominated by the reaction of RO+O<sub>2</sub>, accounting for ~90% of the total production rate. Further

---

classification of RO+O<sub>2</sub> pathway suggested that the oxidation of CH<sub>3</sub>O made a significant contribution of ~47%, followed by RO (from isoprene) + O<sub>2</sub> reaction (12%) and RO (from aromatics) + O<sub>2</sub> reaction (~11%). This result is comparable to the study of (Yang et al., 2020; Yang et al., 2018). It is notable that the reaction of RO (from aromatics) + O<sub>2</sub> could become the predominant pathway of HCHO production during nighttime. This could be attributed to the high level of NO<sub>3</sub> during nighttime, by which styrene could be quickly oxidized and generate N-containing RO radicals, and furtherly generate HCHO. During daytime, isoprene became the most important VOC specie of HCHO production, with a mean rate of 0.48 ppbv h<sup>-1</sup>. As mentioned, this site is surrounded by highly vegetated areas, which can provide abundant biogenic isoprene. During daytime, over 90% of isoprene was oxidized by OH radicals (Figure S4). According to MCMv3.3.1, several RO<sub>2</sub> species (e.g. ISOP34O<sub>2</sub>, ISOPDO<sub>2</sub>, ISOPCO<sub>2</sub>, CISOPAO<sub>2</sub>, ISOPAO<sub>2</sub>) can be generated during the OH-initiated degradation process of isoprene (Jenkin et al., 2015). With the present of NO, isoprene-originated RO<sub>2</sub> can transfer into RO (e.g. ISOPDO, ISOP34O, ISOPAO). The subsequent degradation processes of isoprene-related RO, especially ISOP34O, ISOPDO, ISOPAO and ISOPBO, are tightly related to the formation of HCHO (Jenkin et al., 2015). Other sources of HCHO, such as the reaction between VOC and O<sub>3</sub>, photolysis of OVOC and the reaction of OVOC+OH only contributed minor amount of the total production rate during whole day.

As for HCHO depletion, the photolysis of HCHO and the reaction of HCHO+OH was the two dominate pathways, accounting for ~52% and ~48% of the total depletion rate, respectively. The net HCHO production rate (equals to P(HCHO) + L(HCHO)) was also shown in Figure 8. After sunrise, the net production rate of HCHO raised gradually until 8:00, when it reached the maximum rate (1.6 ppbv h<sup>-1</sup>). This result is comparable to the study of Yang et al. (2018). At around 12:00, the net(HCHO) dropped to ~0 ppbv h<sup>-1</sup>, that was roughly consistent with our observation, which shows that the HCHO peak occurs at around 12:00. Between 13:00 and

14:00, a negative net(HCHO) was found. Although the reaction of RO+O<sub>2</sub> quickly produced HCHO at afternoon, the depletion pathways, especially the photolysis of HCHO, became more competitive, leading to the net reduction of HCHO. This also indicated that strong photochemical reactions do not monotonously profit the accumulation of HCHO, it can also constrain high HCHO levels in certain situations. After 14:00, the photolysis of HCHO dropped rapidly and the net depletion of HCHO back to ~0 ppbv h<sup>-1</sup> at around 15:00. The daytime net HCHO production rate was 0.70 ppbv h<sup>-1</sup>, which was comparable to result of Yang et al. (2018).

The above analysis indicates that the photolysis of OVOC, HCHO, O<sub>3</sub> and HONO was the primary source of RO<sub>x</sub>, which offers high oxidizing environment for the degradation of VOCs. As a typical by-product in the degradation of several VOCs, HCHO can be quickly formatted during daytime. The insight into detailed photochemical processes shows the important role of isoprene in the formation of HCHO.

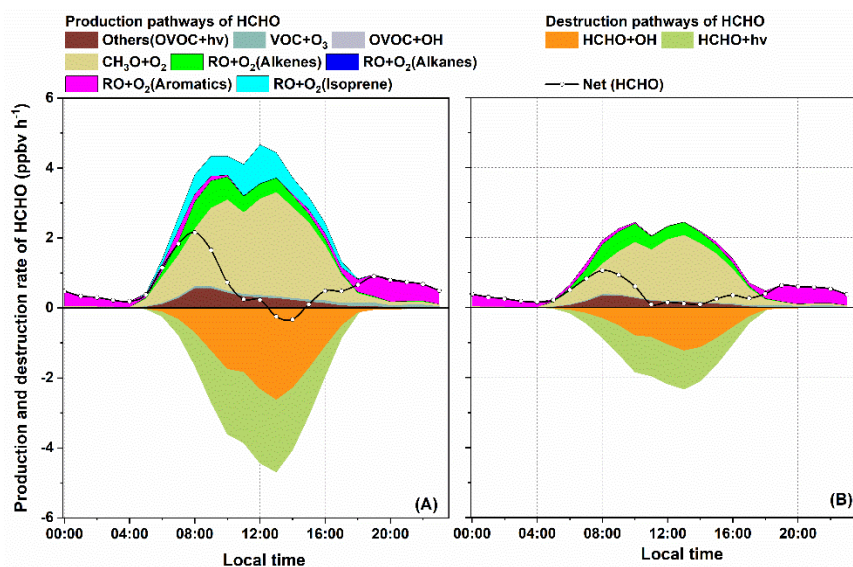


Figure 8. Simulated average diurnal profiles of net rate (net (HCHO)), breakdown HCHO production rate and sink rate (ppbv h<sup>-1</sup>) in S0 (A) and S1 (B).

### 3.6 Impacts of isoprene chemistry on photochemistry

#### 3.6.1 Impact on RO<sub>x</sub> budget

As aforementioned, the degradation of isoprene is tightly related to the cycling of RO<sub>x</sub>. To roughly explain the impact of isoprene chemistry on RO<sub>x</sub> budget, we carried out a parallel

simulation (S1) where isoprene chemistry is disabled (see in Figure 9). The diurnal variation of OH, HO<sub>2</sub>, RO<sub>2</sub> and NO<sub>3</sub> in S1 is also shown in Figure 4 (B) which clearly suggests the decline in RO<sub>x</sub> and NO<sub>3</sub> without isoprene input. To investigate the underlying causes, we calculated the production rate of RO<sub>x</sub> (P(RO<sub>x</sub>)) and loss rate of RO<sub>x</sub> (L(RO<sub>x</sub>)) in S1, respectively (Figure 5 (B)). From the comparison, we found most of the reaction rates in P(RO<sub>x</sub>) and L(RO<sub>x</sub>) showed a decrease trend in S1, suggesting that the absence of isoprene slows down the RO<sub>x</sub> recycling. The photolysis of OVOC (0.67 ppbv h<sup>-1</sup>) is still the predominant primary source of RO<sub>x</sub>. However, without isoprene, the photolysis rate of OVOC decreased by 0.49 ppbv h<sup>-1</sup>. The total production and depletion rate of OH dropped to 6.96 and 7.51 ppbv h<sup>-1</sup>, respectively. Although the absence of isoprene could reduce the consumption of OH, the OH concentration would be reduced by ~16% compared to S0, suggesting that the amount of OH produced via isoprene chemistry is large enough to compensate for the shift from OH to peroxy radicals in the RO<sub>x</sub> family. As for RO<sub>2</sub>, the daytime production and sink rate falls to 3.25 and 3.34 ppbv h<sup>-1</sup>, respectively. This means the concentration of RO<sub>2</sub> would be in a stage of gradual decrease. In addition, the absence of isoprene could also reduce RO<sub>2</sub> concentration by ~20%, suggesting that isoprene was an important source of RO<sub>2</sub> at DSL site. As for HO<sub>2</sub>, drastic decrease of ~53% was found in S1. The above-mentioned decrease in RO<sub>x</sub> obviously could not be explained solely by the remove of isoprene-related radicals. Inspection of the model results shows that OVOC concentrations decreased drastically (~41%) after cutting isoprene (e.g. ~37% decrease in formaldehyde, ~65% decrease in methylglyoxal, ~51% decrease in glyoxal, ~100% decrease in methacrolein (MACR), and ~100% decrease in methyl vinyl ketone (MVK)). The decrease in OVOC can further pull down substantial amount of primary RO<sub>2</sub> and HO<sub>2</sub> (Figure 6 and Figure 9). It is interesting to note that, subtracting isoprene also cause drop of NO<sub>3</sub> (~23%). This result can be contributed to the decrease of secondary production of O<sub>3</sub> (~35%), which can further reduce the formation of NO<sub>3</sub>, especially during nighttime.



(0.265 ppbv h<sup>-1</sup>). Apparently, the absence of isoprene will reduce the total concentrations of alkenes and can further leads to the decrease of RO<sub>2</sub> and OH level, which ultimately slows down the depletion pathways of O<sub>3</sub>. Eventually, the absence of isoprene caused a decrease of 5.78 ppbv h<sup>-1</sup> in the daytime mean net production rate of O<sub>3</sub>. Hence, isoprene chemistry plays an important role in the local O<sub>3</sub> formation at DSL site.

### 3.6.3 Impact on HCHO formation

The analysis of S0 revealed the important role of isoprene, aromatics, and alkenes in the production of HCHO. To investigate the chain effect of isoprene chemistry on HCHO production, the major reactions that dominate the formation and depletion of HCHO in S1 were also analyzed by OBM model (see Figure 8 (B)). Comparison of S0 and S1 shows that the daily average HCHO decreased by 2.90 ppbv (~39%) when cutting away isoprene chemistry. It is obviously that the drop in HCHO concentration cannot be solely illustrated by the absence of RO (from isoprene). As aforementioned, the absence of isoprene slows down the recycling of RO<sub>x</sub> and can further lead to decrease in RO<sub>x</sub> concentration. According to the result of OBM analysis, the concentration of CH<sub>3</sub>O, RO (from aromatics), RO (from alkanes), and RO (from alkenes) decreased by 2.70×10<sup>2</sup> molecule cm<sup>-3</sup>, 1.59×10<sup>5</sup> molecule cm<sup>-3</sup>, 3.35×10<sup>1</sup> molecule cm<sup>-3</sup>, and 3.44 molecule cm<sup>-3</sup>, respectively. The drop in the HCHO precursor concentrations ultimately lead to decrease in the daytime reaction rate of CH<sub>3</sub>O + O<sub>2</sub>, RO (from alkenes) + O<sub>2</sub>, and RO (from aromatics) + O<sub>2</sub> decreased by 0.66 ppbv h<sup>-1</sup> (~36%), 0.06 ppbv h<sup>-1</sup> (~16%), and 0.06 ppbv h<sup>-1</sup> (~40%), respectively. The total daytime formation rate of HCHO dropped to 1.71 ppbv h<sup>-1</sup>, which was 1.66 ppbv h<sup>-1</sup> (~49%) lower than that in S0. As a result of the lower HCHO and OH concentration in S1, the daily mean depletion rate of HCHO decreased by 1.25 ppbv h<sup>-1</sup> (~49%). Finally, the absence of isoprene pulls down the daily average HCHO level by 1.61ppbv (~36%).



---

## 4. Conclusions

Our observations at a suburban site of the YRD region from April to June in 2018 captured 5 typical local O<sub>3</sub> formation episodes. The detailed atmospheric photochemistry during these episodes were analyzed. Under stagnant condition, the photolysis of OVOC served as the predominant primary RO<sub>x</sub> sources. RO<sub>x</sub> achieves efficient recycling with the participation of NO<sub>x</sub>. Influenced by the fast RO<sub>x</sub> recycling, local O<sub>3</sub> was efficiently produced and accumulated under stagnant conditions. The reactions of RO radicals with O<sub>2</sub> dominate the photochemical formation of HCHO. The higher atmospheric oxidative capacity lead to fast degradation of VOCs, which can further lead to high levels of HCHO at the DSL site. Specifically, the degradation of RO radicals (e.g. ISOP34O, ISOPDO, ISOPAO and ISOPBO) from isoprene oxidation play an important role in the photochemical production of HCHO. To investigate the role of isoprene in RO<sub>x</sub> recycle and the formation of secondary pollutant, a sensitivity scenario without isoprene (S1) input was simulated by OBM model. By comparing S1 to the standard simulation (S0), we find that isoprene chemistry is important to local RO<sub>x</sub> recycling. The absence of isoprene can obviously decrease the concentrations of OVOC and the reaction rates in RO<sub>x</sub> propagations, and further reduce the concentrations of radicals (e.g. OH, HO<sub>2</sub>, RO<sub>2</sub>). Our results indicate that the isoprene chemistry can strongly influence the formation of O<sub>3</sub> and HCHO with the present of NO<sub>x</sub>. Removing isoprene can slow down the reaction of HO<sub>2</sub>+NO and RO<sub>2</sub>+NO by ~37% and ~45%, respectively, and eventually cause ~34% decrease of O<sub>3</sub>. As a result of lower O<sub>3</sub> concentration, average concentration of NO<sub>3</sub> dropped by 23% in S1. The absence of isoprene can lead to decrease of RO (from isoprene) and RO<sub>x</sub> concentration and cause an obvious drop of HCHO formation (~49%). Overall, this study underlines the significant role of isoprene chemistry in radical chemistry, photochemical reactions, and secondary pollutant formation in the atmosphere of the YRD region and provides insights into secondary pollution and its formation mechanisms.

---

*Data availability.* The data that support the results are available from the corresponding author upon request.

*Authorship contribution.* Kun Zhang: Formal analysis, Methodology, Writing-original draft. Ling Huang: Writing-review. Qing Li: Formal analysis. Juntao Huo: Formal analysis, Data curation. Yusen Duan: Formal analysis, Data curation. Yuhang Wang: Writing-review. Yangjun Wang: Formal analysis. Qingyan Fu: Formal analysis. Li Li: Conceptualization, Methodology, Writing-review & editing.

*Competing interest.* The authors declare that they have no known competing financial interests or personal relationships that could have appeared to influence the work reported in this paper.

*Acknowledgements.* This study is supported by the National Natural Science Foundation of China (No.4185161), Shanghai International Science and Technology Cooperation Fund (No. 19230742500), and Shanghai Science and Technology Fund (No. 19DZ1205007). Y. Wang was supported by the National Science Foundation. We thank Shanghai Environmental Monitoring Center (SEMC) for conducting the measurement and sharing the data.

*Financial support.* This study was financially supported by the National Natural Science Foundation of China (NO. 41875161; NO.42075144), Shanghai International Science and Technology Cooperation Fund (NO. 19230742500), Shanghai Science and Technology Fund (No. 19DZ1205007), Shanghai Sail Program (NO.19YF1415600), and the National Key



---

Research and Development Program of China (NO.2018YFC0213600). Y. Wang was supported by the National Science Foundation.

## References

- Atkinson, R., and Arey, J.: Atmospheric degradation of volatile organic compounds, *Chemical reviews*, 103, 4605-4638, 2003.
- Atkinson, R., Baulch, D. L., Cox, R. A., Crowley, J. N., Hampson, R. F., Hynes, R. G., Jenkin, M. E., Rossi, M. J., and Troe, J.: Evaluated kinetic and photochemical data for atmospheric chemistry: Volume II - Gas phase reactions of organic species, *Atmospheric Chemistry and Physics*, 6, 3625-4055, 10.5194/acp-6-3625-2006, 2006.
- Chan, K. L., Wang, S. S., Liu, C., Zhou, B., Wenig, M. O., and Saiz-Lopez, A.: On the summertime air quality and related photochemical processes in the megacity Shanghai, China, *Science of the Total Environment*, 580, 974-983, 2017.
- D'Ambro, E. L., Møller, K. H., Lopez-Hilfiker, F. D., Schobesberger, S., Liu, J., Shilling, J. E., Lee, B. H., Kjaergaard, H. G., and Thornton, J. A.: Isomerization of second-generation isoprene peroxy radicals: Epoxide formation and implications for secondary organic aerosol yields, *Environmental science & technology*, 51, 4978-4987, 2017.
- Gong, D., Wang, H., Zhang, S., Wang, Y., Liu, S. C., Guo, H., Shao, M., He, C., Chen, D., He, L., Zhou, L., Morawska, L., Zhang, Y., and Wang, B.: Low-level summertime isoprene observed at a forested mountaintop site in southern China: implications for strong regional atmospheric oxidative capacity, *Atmospheric Chemistry and Physics*, 18, 14417-14432, 10.5194/acp-18-14417-2018, 2018.
- He, Z. R., Wang, X. M., Ling, Z. H., Zhao, J., Guo, H., Shao, M., and Wang, Z.: Contributions of different anthropogenic volatile organic compound sources to ozone formation at a

---

receptor site in the Pearl River Delta region and its policy implications, *Atmospheric Chemistry and Physics*, 19, 8801-8816, 2019.

Jenkin, M. E., Young, J. C., and Rickard, A. R.: The MCM v3.3.1 degradation scheme for isoprene, *Atmospheric Chemistry and Physics*, 15, 11433-11459, 10.5194/acp-15-11433-2015, 2015.

Li, X., Rohrer, F., Brauers, T., Hofzumahaus, A., Lu, K., Shao, M., Zhang, Y. H., and Wahner, A.: Modeling of HCHO and CHOCHO at a semi-rural site in southern China during the PRIDE-PRD2006 campaign, *Atmospheric Chemistry and Physics*, 14, 12291-12305, 10.5194/acp-14-12291-2014, 2014.

Lin, H., Wang, M., Duan, Y., Fu, Q., Ji, W., Cui, H., Jin, D., Lin, Y., and Hu, K.: O<sub>3</sub> sensitivity and contributions of different nmhc sources in O<sub>3</sub> formation at urban and suburban sites in Shanghai, *Atmosphere*, 11, 1-18, 10.3390/atmos11030295, 2020.

Liu, X., Lyu, X., Wang, Y., Jiang, F., and Guo, H.: Intercomparison of O<sub>3</sub> formation and radical chemistry in the past decade at a suburban site in Hong Kong, *Atmospheric Chemistry and Physics*, 19, 5127-5145, 10.5194/acp-19-5127-2019, 2019.

Liu, Y. J., Herdlinger-Blatt, I., McKinney, K. A., and Martin, S. T.: Production of methyl vinyl ketone and methacrolein via the hydroperoxyl pathway of isoprene oxidation, *Atmospheric Chemistry and Physics*, 13, 5715-5730, 10.5194/acp-13-5715-2013, 2013.

Liu, Z., Wang, Y., Gu, D., Zhao, C., Huey, L. G., Stickel, R., Liao, J., Shao, M., Zhu, T., Zeng, L., Amoroso, A., Costabile, F., Chang, C. C., and Liu, S. C.: Summertime photochemistry during CAREBeijing-2007: RO<sub>x</sub> budgets and O<sub>3</sub> formation, *Atmospheric Chemistry and Physics*, 12, 7737-7752, 2012.

Riedel, T. P., Wolfe, G. M., Danas, K. T., Gilman, J. B., Kuster, W. C., Bon, D. M., Vlasenko, A., Li, S.-M., Williams, E. J., Lerner, B. M., Veres, P. R., Roberts, J. M., Holloway, J. S., Lefer, B., Brown, S. S., and Thornton, J. A. (2014). An MCM modeling study of nitryl

---

chloride (ClNO<sub>2</sub>) impacts on oxidation, ozone production and nitrogen oxide partitioning in polluted continental outflow, *Atmos. Chem. Phys.*, 14, 3789–3800, <https://doi.org/10.5194/acp-14-3789-2014>.

Tan, Z. F., Lu, K. D., Jiang, M. Q., Su, R., Wang, H. L., Lou, S. R., Fu, Q. Y., Zhai, C. Z., Tan, Q. W., Yue, D. L., Chen, D. H., Wang, Z. S., Xie, S. D., Zeng, L. M., and Zhang, Y. H.: Daytime atmospheric oxidation capacity in four Chinese megacities during the photochemically polluted season: a case study based on box model simulation, *Atmospheric Chemistry and Physics*, 19, 3493–3513, 2019.

Wennberg, P. O., Bates, K. H., Crounse, J. D., Dodson, L. G., McVay, R. C., Mertens, L. A., Nguyen, T. B., Praske, E., Schwantes, R. H., Smarte, M. D., St Clair, J. M., Teng, A. P., Zhang, X., and Seinfeld, J. H.: Gas-phase reactions of isoprene and its major oxidation products, *Chemical Reviews*, 118, 3337–3390, 2018.

Wolfe, G. M., Kaiser, J., Hanisco, T. F., Keutsch, F. N., de Gouw, J. A., Gilman, J. B., Graus, M., Hatch, C. D., Holloway, J., Horowitz, L. W., Lee, B. H., Lerner, B. M., Lopez-Hilfiker, F., Mao, J., Marvin, M. R., Peischl, J., Pollack, I. B., Roberts, J. M., Ryerson, T. B., Thornton, J. A., Veres, P. R., and Warneke, C.: Formaldehyde production from isoprene oxidation across NO<sub>x</sub> regimes, *Atmospheric Chemistry and Physics*, 16, 2597–2610, [10.5194/acp-16-2597-2016](https://doi.org/10.5194/acp-16-2597-2016), 2016a.

Wolfe, G. M., Marvin, M. R., Roberts, S. J., Travis, K. R., and Liao, J.: The Framework for 0-D Atmospheric Modeling (F0AM) v3.1, *Geoscientific Model Development*, 9, 3309–3319, [10.5194/gmd-9-3309-2016](https://doi.org/10.5194/gmd-9-3309-2016), 2016b.

Xue, L., Wang, T., Gao, J., Ding, A., Zhou, X., Blake, D. R., Fang, X., Saunders, S. M., Fan, S., Zuo, H., Zhang, Q., Wang, W. Ground-level ozone in four Chinese cities: precursors, regional transport and heterogeneous processes. *Atmospheric chemistry and physics*, 14(23), 13175–13188, 2014.

---

571 Xue, L., Gu, R., Wang, T., Wang, X., Saunders, S., Blake, D., Louie, P. K. K., Luk, C. W. Y.,  
572 Simpson, I., Xu, Z., Wang, Z., Gao, Y., Lee, S., Mellouki, A., and Wang, W.: Oxidative  
573 capacity and radical chemistry in the polluted atmosphere of Hong Kong and Pearl River  
574 Delta region: Analysis of a severe photochemical smog episode, *Atmospheric Chemistry  
575 and Physics*, 16, 9891-9903, 10.5194/acp-16-9891-2016, 2016.

576 Yang, X., Xue, L. K., Wang, T., Wang, X. F., Gao, J., Lee, S. C., Blake, D. R., Chai, F. H., and  
577 Wang, W. X.: Observations and explicit modeling of summertime carbonyl formation in  
578 Beijing: identification of key precursor species and their impact on atmospheric oxidation  
579 chemistry, *Journal of Geophysic Research:Atmosphere*, 123, 1426-1440, 2018.

580 Yang, X., Zhang, G. Q., Sun, Y. M., Zhu, L., Wei, X. F., Li, Z., and Zhong, X. L.: Explicit  
581 modeling of background HCHO formation in southern China, *Atmospheric Research*, 240,  
582 UNSP 10494110.1016/j.atmosres.2020.104941, 2020.

583 Zeng, P., Lyu, X. P., Guo, H., Cheng, H. R., Wang, Z. W., Liu, X. F., and Zhang, W. H.: Spatial  
584 variation of sources and photochemistry, of formaldehyde in Wuhan, Central China,  
585 *Atmospheric Environment*, 214, 2019.

586 Zhang, K., Zhou, L., Fu, Q., Yan, L., Bian, Q., Wang, D., and Xiu, G.: Vertical distribution of  
587 ozone over Shanghai during late spring: A balloon-borne observation, *Atmospheric  
588 environment*, 208, 48-60, 2019.

589 Zhang, K., Li, L., Huang, L., Wang, Y., Huo, J., Duan, Y., Wang, Y., and Fu, Q.: The impact  
590 of volatile organic compounds on ozone formation in the suburban area of Shanghai,  
591 *Atmospheric Environment*, 232, 10.1016/j.atmosenv.2020.117511, 2020a.

592 Zhang, K., Xu, J., Huang, Q., Zhou, L., Fu, Q., Duan, Y., and Xiu, G.: Precursors and potential  
593 sources of ground-level ozone in suburban Shanghai, *Frontiers of Environmental Science  
594 and Engineering*, 14, 10.1007/s11783-020-1271-8, 2020b.

---

Zhu, J., Cheng, H., Peng, J., Zeng, P., Wang, Z., Lyu, X., and Guo, H.: O<sub>3</sub> photochemistry on O<sub>3</sub> episode days and non-O<sub>3</sub> episode days in Wuhan, Central China, *Atmospheric Environment*, 223, 10.1016/j.atmosenv.2019.117236, 2020a.

Zhu, J., Wang, S. S., Wang, H. L., Jing, S. G., Lou, S. R., Saiz-Lopez, A., and Zhou, B.: Observationally constrained modeling of atmospheric oxidation capacity and photochemical reactivity in Shanghai, China, *Atmospheric Chemistry and Physics*, 20, 1217-1232, 2020b.

Zong, R. H., Yang, X., Wen, L., Xu, C. H., Zhu, Y. H., Chen, T. S., Yao, L., Wang, L. W., Zhang, J. M., Yang, L. X., Wang, X. F., Shao, M., Zhu, T., Xue, L. K., and Wang, W. X.: Strong ozone production at a rural site in the North China Plain: Mixed effects of urban plumes and biogenic emissions, *Journal of Environmental Sciences*, 71, 261-270, 10.1016/j.jes.2018.05.003, 2018.